THE JOURNAL OF PHYSICAL CHEMISTRY C

Article

pubs.acs.org/JPCC

First-Principles Study of Methanol Oxidation into Methyl Formate on Rutile TiO_2(110)

Xiufeng Lang,[†,∥] Bo Wen,[†,§] Chuanyao Zhou,[‡] Zefeng Ren,[§] and Li-Min Liu*[,†]

[†]Beijing Computational Science Research Center, Beijing, 100084 China

[‡]State Key Laboratory of Molecular Reaction Dynamics, Dalian Institute of Chemical Physics, Chinese Academy of Science, 457 Zhongshan Road, Dalian, 116023 Liaoning China

[§]International Center for Quantum Materials (ICQM) and School of Physics, Peking University, Beijing, 100871 China

[∥]Department of Physics, Hebei Normal University of Science & Technology, Qinghuangdao, 066004 China

ABSTRACT: The detailed oxidation of methanol into methyl formate on perfect and defect rutile TiO_2(110) surfaces was explored based on first-principles calculations. Based on the calculated energy barriers of elementary steps, a pathway was identified for methanol oxidation on both surfaces. The reaction proceeds through a direct coupling of methoxy and formaldehyde to produce the intermediate hemiacetal, which leads to methyl formate. Kinetics of elementary steps further shows that methanol dissociation at surface oxygen vacancy greatly changes the reaction rates of the sequential reaction steps on the defect surface, making them quite different from those occurring at the Ti_{5c} sites on both surfaces. In addition, small diffusion barriers of formaldehyde demonstrate that it can move freely from the adsorption sites to the reactive sites on the surfaces to produce the hemiacetal. These findings may provide insights into the complete oxidation mechanism for methanol on TiO_2, and demonstrate a green and benign route for the synthesis of ester directly from alcohols or from alcohols and aldehydes.

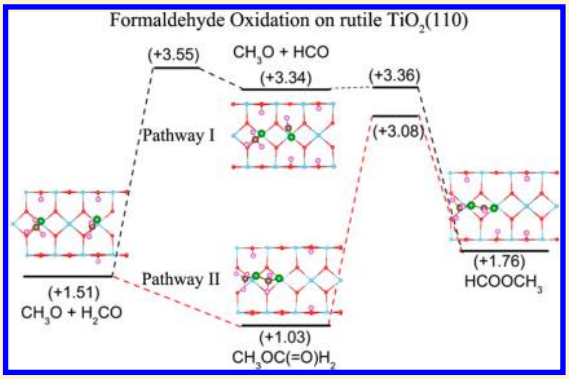

1. INTRODUCTION

Titanium dioxide (TiO_2) has been extensively investigated as a catalyst or photocatalyst, particularly in applications involving photodegradation of organic molecules and water photosplitting.[1−3] Simple alcohols are often used as model systems of thermal and photocatalytic oxidation of organic contaminants on TiO_2.[4−8] Among them, photochemistry of methanol (CH_3OH) on TiO_2 has been widely studied under a variety of conditions because CH_3OH as a hole scavenger greatly enhances the activity of TiO_2 in photocatalytic splitting of water into hydrogen.[9−12] Many studies on selective oxidation of methanol over TiO_2 photocatalysts have been carried out, and various products, such as H_2, CO_2, H_2CO, HCOOH, and $HCOOCH_3$, have been suggested.[9,13,14]

The rutile TiO_2(110) surface is a model substrate,[15−19] and many experimental and theoretical studies have been performed to study the thermal chemistry of CH_3OH on the substrate. Both molecular and dissociative forms of CH_3OH have been reported on the TiO_2(110) surface by temperature-programmed desorption (TPD) and scanning tunneling microscopy (STM) methods, with its dissociation occurring primarily at bridging oxygen vacancies (V_O's) and steps of the surface, but arguments still exist on whether CH_3OH can thermally dissociate on the 5-fold coordinated titanium (Ti_{5c}) sites.[10,20−23] Recently, the photochemistry of CH_3OH at the Ti_{5c} sites on the TiO_2(110) surface has been explored experimentally.[24−30] For example, Henderson et al. compared the TPD spectra from CH_3OH and methoxy (CH_3O) on TiO_2(110) after ultraviolet irradiation and suggested that CH_3OH on the preoxidized TiO_2(110) surface should be thermally dissociated into the active CH_3OH, which can be then photocatalyzed into formaldehyde (H_2CO) species.[25] Yang et al. further reported that molecularly chemisorbed CD_3OD on the reduced TiO_2(110) undergoes a stepwise photocatalytic dissociation to form D_2CO species by observing the TPD spectra from deuterated methanol (CD_3OD) on TiO_2(110) after the laser irradiation.[26] Considering the rich photochemistry of CH_3OH on TiO_2-based catalysts, Friend et al. examined the reaction by comparing the TPD spectra and STM images of CH_3OH on the preoxidized TiO_2(110) with and without laser irradiation and demonstrated first sequential photo-oxidation of CH_3OH into methyl formate ($HCOOCH_3$) on the surface.[29] They proposed that a transient formyl (HCO) was produced in the secondary photo-oxidation of H_2CO and then transformed into $HCOOCH_3$. However, Yang et al. used TPD measurements of isotopic substitution to show that DCO produced from the laser irradiation of D_2CO cannot be an intermediate in the cross-coupling reaction that produce $DCOOCD_3$ and suggested that the reaction probably proceeds through an intermediate hemiacetal ($CH_3OC(=O)H_2$) rather

Received: June 7, 2014
Revised: August 1, 2014
Published: August 11, 2014

dx.doi.org/10.1021/jp505674g | J. Phys. Chem. C 2014, 118, 19859−19868

than an intermediate HCO.[28] Huang et al.[30] also gave direct spectroscopic evidence for the formation of $HCOOCH_3$ as the product of photocatalytic dissociation of $CH_3OC(=O)H_2$ by using TPD spectra and X-ray photoelectron spectroscopy (XPS) of CH_3OH on the reduced $TiO_2(110)$ after laser irradiation. The lack of consistency in these findings clearly indicates the need for a thorough investigation on the photo-oxidation mechanism of CH_3OH into $HCOOCH_3$ on the $TiO_2(110)$. Theoretically, many studies have explored the oxidation mechanism of water, ethylene glycol, and phenylmethanol on TiO_2 under thermal or photocatalytic conditions.[5,7,31−34] However, few studies on mechanism of CH_3OH oxidation into $HCOOCH_3$ under thermal or photocatalytic conditions has been reported.[23,35,36] In this work, we would address oxidation pathways of CH_3OH on the $TiO_2(110)$ under thermal condition.

All these TPD, STM, and XPS experiments observed the photo-oxidation of CH_3OH into $HCOOCH_3$ on the $TiO_2(110)$ surface happening at the Ti_{5c} sites not at the V_O's sites. This is quite different from the fact that the V_O's were often regarded as the active reaction sites for catalysis and photocatalysis of the TiO_2-based materials. To our knowledge, there are only several reports on the effects of V_O's on the thermally or photo driven dissociation of CH_3OH into CH_3O on the reduced $TiO_2(110)$.[23,35,37] For example, Zhou et al.[37] investigated photocatalytic dissociation of deuterated methanol (CD_3OD) on both stoichiometric and reduced $TiO_2(110)$ surfaces using time-dependent two-photon photoemission (2PPE) methods, and demonstrated that the dissociation kinetics on the reduced surface was greatly enhanced as compared to that on the stoichiometric surface. Up to date, the detailed study on the roles of V_O's in the overall oxidation process of CH_3OH is still rare.

In this paper, the intrinsic mechanism of the CH_3OH oxidation into $HCOOCH_3$ on both perfect and defect $TiO_2(110)$ was systematically explored based on first-principles calculations. The kinetics of all relevant elementary steps in the oxidation process was carefully investigated. The calculation results suggest that reaction kinetics of the elementary steps can clarify the $CH_3OC(=O)H_2$/HCO selectivity to produce the final species $HCOOCH_3$ on the perfect and defect $TiO_2(110)$.

2. THEORETICAL METHODS

Electronic structure calculations were performed within the framework of density functional theory (DFT), as implemented in the Vienna ab initio simulation program (VASP), a plane-wave pseudopotential package.[38] The exchange and correlation energies were calculated using the Perdew, Burke, and Ernzerhof (PBE) functional within the generalized gradient approximation (GGA).[39] The projector augmented-wave method (PAW)[40] was employed to treat valence-core interactions with 12, 4, and 6 valence electrons for Ti, C, and O, respectively. All surface reactions were modeled on a (4×2) rutile-$TiO_2(110)$ surface slab, which contains 4 TiO_2 trilayers and a 15 Å thick vacuum layer. To model the surface reactions on the defect $TiO_2(110)$ surface, one bridging oxygen atom (O_{br}) was removed from the surface slab, and thus the system represents a surface with a 12.5% oxygen vacancy concentration, approaching the vacancy concentration of 10% observed in experiments.[41] During structure optimization, the adsorbates and the three top TiO_2 trilayers were allowed to relax in all directions while the bottom TiO_2 trilayer was fixed at the optimized bulk position. A plane-wave cutoff energy of 400 eV was used. The relaxation of the atoms was carried out until the force on any atom was less than 0.03 eV $Å^{-1}$. The criterion for the total energy was set as 1×10^{-5} eV. Based on the optimized structures for the initial and final states in each elementary step, minimum energy paths and corresponding activation barriers were calculated using the climbing image nudged elastic band approach (CI-NEB).[42,43] The minimum energy path is examined using 7−10 images, including the initial and final states, during the transition state search. Note that stable structure locations of all adsorbed species on the perfect and defect $TiO_2(110)$ were reported by taking into account of both the energy stability and structure appropriate for reaction to occur.

3. RESULTS AND DISCUSSION

The overall oxidation process of CH_3OH on the $TiO_2(110)$ was investigated by DFT calculations. In this work, the typical adsorption site of the CH_3OH is the Ti_{5c} on the surface. Two CH_3OH molecules are considered with the (4×2) $TiO_2(110)$, which corresponds to 1/4 monolayer (ML). According to previous studies about $HCOOCH_3$ production from CH_3OH, the reaction may occur via three possible mechanisms depending on the different intermediates. The first way needs to generate an intermediate $(H_2CO)_2$,[9] called the Tishchenko mechanism, the second one requires the intermediate $CH_3OC(=O)H_2$,[44] known as the hemiacetal mechanism, and the last mechanism needs the intermediate HCO, called the formyl mechanism.[29] As for the Tishchenko mechanism, TPD experiments suggested that no formaldehyde oligomers, $(H_2CO)_n$, desorption was observed on the $TiO_2(110)$[29,45,46] and thus cannot produce $HCOOCH_3$ on the perfect $TiO_2(110)$. Furthermore, the $(H_2CO)_2$ adsorption geometries on the perfect and defect $TiO_2(110)$ were also investigated in this work. Interestingly, the initial dimer structure is rather unstable, and it automatically separates into two single H_2CO during the structure relaxation. Thus, $HCOOCH_3$ production from CH_3OH by the Tishchenko mechanism is not considered, and we only consider the two other mechanisms of $HCOOCH_3$ production with the intermediates $CH_3OC(=O)H_2$ and HCO in the following. The typical products of the CH_3OH oxidation are CH_3O, H_2CO, HCO, $CH_3OC(=O)H_2$, and $HCOOCH_3$ in these two mechanisms. In this work, the effect of surface holes is not considered; thus, the detailed mechanism of CH3OH oxidation may be changed under the photocatalytic situations.

3.1. Pathway of Methanol Oxidation on the Perfect $TiO_2(110)$. *3.1.1. Adsorption of Methanol and Its Oxidation Products.* For the perfect surface, the stable geometries for CH_3OH, CH_3O, H_2CO, HCO, $CH_3OC(=O)H_2$, and $HCOOCH_3$ are shown in Figure 1, and the corresponding Ti−O bond lengths are listed in Table 1. As for the optimized geometries, the oxygen atoms of methanol molecules are adsorbed at the Ti_{5c} sites and the hydrogen atoms are pointing to the nearby bridging oxygen atoms (O_{br}). The adsorption geometry of the methoxy is quite similar to that of the methanol, as reported in the previous theoretical calculations.[21,23] The main differences are that the proton of the hydroxyl transfers to the O_{br} and the CH_3 group has a small tilt to the normal line of the $TiO_2(110)$ surface.

The H_2CO is adsorbed on the surface with the CH_2 group pointing diagonally to the bridging oxygen rows in the [001] direction. The HCO molecule adopts a stable configuration where the molecular plane is vertical to the bridging oxygen

dx.doi.org/10.1021/jp505674g | J. Phys. Chem. C 2014, 118, 19859−19868

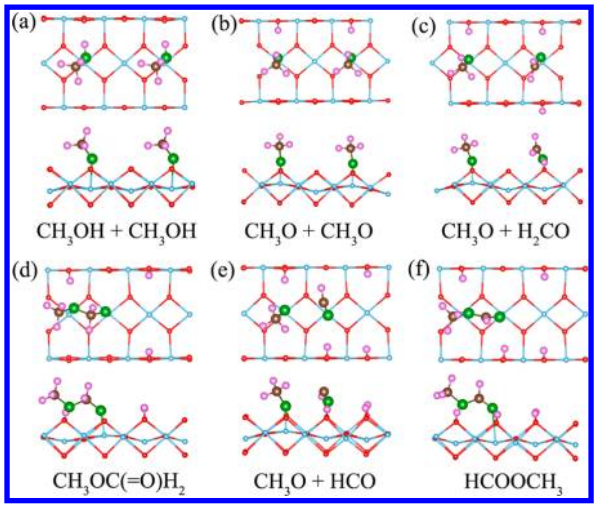

Figure 1. Top and side views of optimized adsorption structures for (a) CH_3OH, (b) CH_3O, (c) CH_3O and H_2CO, (d) $CH_3OC(=O)H_2$, (e) CH_3O and HCO, and (f) $HCOOCH_3$ on the perfect $TiO_2(110)$-(4×2) surface unit cell. The red and green represent the O atoms; light blue, gray and purple balls represent the Ti, C, and H atoms, respectively.

row and its H and O atoms form two hydrogen bonds with the neighboring O_{br} atom and the H atom in the nearby $O_{br}H$, respectively. Both $CH_3OC(=O)H_2$ and $HCOOCH_3$ adopt similar configurations with the molecular skeleton parallel to the bridging oxygen row.

To compare thermodynamic feasibility of the elementary steps involving these species on the $TiO_2(110)$, adsorption energies (E_{ads}) are calculated through a formula: $E_{ads} = 1/2[E_{adsorbate/TiO2} - (E_{TiO2} + 2E_{CH3OH})]$, where E_{TiO2} and E_{CH3OH} are the total energies of the clean $TiO_2(110)$ surface and free CH_3OH molecule, respectively. The data are listed in Table 1. The more negative E_{ads} corresponds to a more stable structure. The calculated E_{ads} is −0.79 eV for CH_3OH, which is in consistent with the previous calculations on the adsorption energies of two CH_3OH adsorbed at two adjacent Ti_{5c} sites on the $TiO_2(110)$.[36] When one of the CH_3OH molecules is dissociated into CH_3O, the adsorption energy per molecule becomes −0.76 eV, which is about 0.03 eV more stable than that of the perfect one. When both CH_3OH molecules are fully dissociated into CH_3O, the adsorption energy becomes −0.59 eV per molecule, which is about 0.2 eV less negative than that of the CH_3OH. The changes of adsorption energies clearly indicates that the dissociation of CH_3OH on the perfect $TiO_2(110)$ is not energetically favorable.

When the CH_3O is further dissociated into H_2CO, the adsorption energy becomes −0.06 eV, which is 0.53 eV less negative than CH_3O, demonstrating the energetically infeasible dissociation of CH_3O. As for one transformation way, when the H_2CO is dissociated into the intermediate species HCO, the adsorption energy increases from −0.06 to 0.87 eV. Thus, it becomes more difficult to further scissor the hydrogen atom from H_2CO into HCO configuration. The CH_3O and HCO can spontaneously combine to produce the final $HCOOCH_3$, with the smaller adsorption energy of $HCOOCH_3$ (0.08 eV). As for the other transformation way, the more negative adsorption energy of $CH_3OC(=O)H_2$ (−0.28 eV) indicates that H_2CO and CH_3O can spontaneously couple into the intermediate species, while the further transformation from $CH_3OC(=O)H_2$ into $HCOOCH_3$ is not energetically favorable. These results clearly indicate that the C−H scissor of CH_3O, H_2CO, and $CH_3OC(=O)H_2$ need the large energies to overcome, so these steps might determine the reaction rate of the overall oxidation process of CH_3OH. In order to known whether the zero-point energy (ZPE) correction is important for this system, several typical adsorption species were further checked considering the ZPE correction. As shown in Table 1, the ZPE correction does not change the trend of the relative stability of each species. This will be further elucidated kinetically by the calculated energy barriers of all elementary steps in the following studies.

3.1.2. Pathways for Methanol Oxidation. After determining the stable adsorption configurations and the adsorption energies of CH_3OH and its oxidation products on the $TiO_2(110)$, the detailed reaction profiles of CH_3OH oxidation into $HCOOCH_3$ on the $TiO_2(110)$ are further explored. For the initial two reaction steps, the CH_3OH is dissociated into CH_3O via the O−H bond cleavage and then dissociated into H_2CO via a C−H scissor, which is described as follows:

$$CH_3OH(a) + O_{br} \rightarrow CH_3O(a) + O_{br}H \quad (1)$$

$$CH_3O(a) + O_{br} \rightarrow H_2CO(a) + O_{br}H \quad (2)$$

Figure 2a illustrates the potential energy profiles of these reaction steps for two CH_3OH molecules, and the calculated results are listed in Table 2. The O−H dissociation step of the first CH_3OH has an energy barrier of 0.35 eV. The atomic configuration of a transition state (TS1) with a strong O_{br}-H bond (1.171 Å) and a weak O−H bond of CH_3OH (1.295 Å) is close to the product of CH_3O. Due to relatively small energy

Table 1. Adsorption Energies (E_{ads}) and Bond Lengths of Ti−O of Methanol and Its Oxidation Products on the Perfect $TiO_2(110)$ (Per.), the Defect $TiO_2(110)$ with Methanol Adsorbed at the Ti_{5c} Sites (Def-Ti_{5c}), and the Defect $TiO_2(110)$ with Methanol Adsorbed at the Ti_{5c} and V_O Sites (Def-V_O)[A]

	Per.			Def-Ti_{5c}			Def-V_O			
	E_{ads} (eV)	Ti−O_1 (Å)	Ti−O_2 (Å)	E_{ads} (eV)	Ti−O_1 (Å)	Ti−O_2 (Å)	E_{ads} (eV)	Ti−O_1 (Å)	Ti−O_2 (Å)	Ti−O_3 (Å)
2 CH_3OH	−0.79 (−0.67)	2.255	2.256	−0.76	2.282	2.263	−0.83	2.383	2.381	2.239
CH_3OH + CH_3O	−0.76 (−0.69)	2.299	1.789	−0.71	2.309	1.805	−1.02	1.978	2.083	2.256
2 CH_3O	−0.59 (−0.56)	1.806	1.804	−0.53	1.826	1.815	−0.98	1.958	2.122	1.792
CH_3O + H_2CO	−0.06	1.813	2.500	0.18	1.825	2.405	−0.18	2.034	2.014	1.914
CH_3O + HCO	0.87	1.835	2.732	0.98	1.804	2.596	0.75	2.056	2.059	
$CH_3OC(=O)H_2$	−0.28	1.852	2.578	−0.08	1.854	2.366	−0.13	2.467	2.589	1.890
$HCOOCH_3$	0.08	2.598	2.925	0.18	2.449	2.727	0.32	2.426		

[A]The adsorption energies with ZPE correction for several species are also calculated, shown in the parentheses.

dx.doi.org/10.1021/jp505674g | J. Phys. Chem. C 2014, 118, 19859−19868

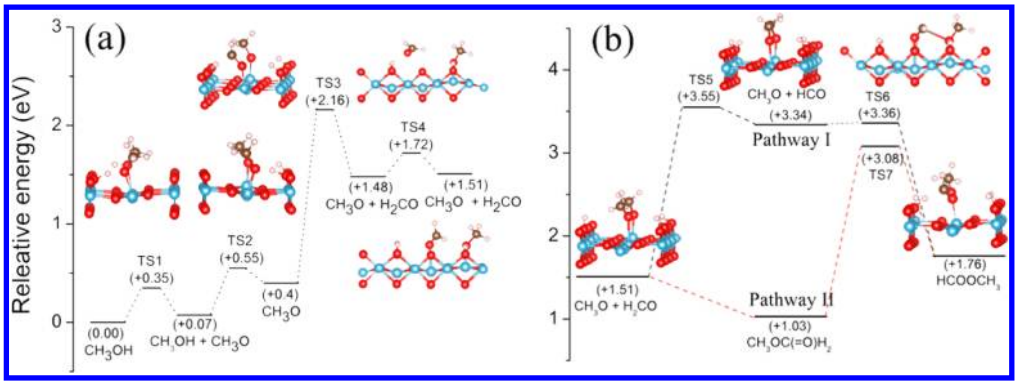

Figure 2. Calculated potential energy profiles for (a) CH_3OH dissociation into H_2CO and (b) H_2CO oxidation into $HCOOCH_3$ on the perfect $TiO_2(110)$ (pathway I and pathway II). The structures of the transition states in each step are embedded, and two side views of mixed H_2CO and CH_3O configurations at two adjacent Ti_{5c} sites are shown in (a) and (b) as well. Note that the energy of each configuration is relative to the total energy of the initial configuration that two CH_3OH molecules adsorb on the $TiO_2(110)$ in (a) and (b). The red, light blue, gray, and white balls in the insets represent the O, Ti, C, and H atoms, respectively.

Table 2. Calculated Energy Barrier and Thermodynamic Energy for Possible Reaction Pathways for Methanol Oxidation on the Perfect $TiO_2(110)$ (Per.), the Defect $TiO_2(110)$ with Methanol Adsorbed at the Ti_{5c} Sites (Def-Ti_{5c}), and the Defect $TiO_2(110)$ with Methanol Adsorbed at the Ti_{5c} and V_O Sites (Def-V_O)

	Per.		Def-Ti_{5c}		Def-V_O	
	E_B[a] (eV)	E_{Tb}[b] (eV)	E_B[a] (eV)	E_{Tb}[b] (eV)	E_B[a] (eV)	E_{Tb}[b] (eV)
$CH_3OH + O_{in} \rightarrow CH_3O + O_{in}H$					0.33	0.05
$O_{in}H + O_{br} \rightarrow O_{br}H + O_{in}$					0.30	−0.43
$CH_3OH + O_{br} \rightarrow CH_3O + O_{br}H$	0.35	0.07	0.34	0.11	0.24	0.03
	0.48	0.33	0.49	0.37		
$CH_3O + O_{br} \rightarrow H_2CO + O_{br}H$	1.76	1.08	1.93	1.42	1.85	1.60
$H_2CO + O_{br} \rightarrow HCO + O_{br}H$	2.04	1.83	1.92	1.66	2.44	2.11
$CH_3O + HCO \rightarrow HCOOCH_3$	0.02	−1.58		−1.59	0.23	−0.85
$CH_3O + H_2CO \rightarrow CH_3OC(=O)H_2$		−0.48	0.07	−0.41	0.45	0.35
$CH_3OC(=O)H_2 + O_{br} \rightarrow HCOOCH_3 + O_{br}H$	2.05	0.73	1.92	0.48	1.94	0.91

[a]The energy barrier (E_B) is defined as the difference between the energy of the transition state (E_{TS}) and the energy of the initial state (E_i); i.e., $E_B = E_{TS} - E_i$. [b]Thermodynamic energy (E_{Th}) is defined as the difference between the energy of the final state (E_f) and the energy of the initial state (E_i); i.e., $E_{Th} = E_f - E_i$.

barrier, the dissociation of CH_3OH into CH_3O should be quite easy. Although the configuration of TS2 is similar to that of TS1, the further dissociation of the second CH_3OH requires a slightly large energy barrier of 0.48 eV compared with the dissociation of the first CH_3OH.

The CH_3O is further dissociated into H_2CO through a hydrogen transfer from the CH_3O to another nearby O_{br} site. The C−H scissor step needs to overcome a large energy barrier of 1.76 eV. The calculated energy barriers of the O−H dissociation step and the C−H scissor steps indicate that CH_3OH dissociation into CH_3O could be easily initiated by thermal excitation at ambient conditions, while the CH_3O dissociation into H_2CO should be initiated by photo excitation, which is in accordance with the previously experimental measurements.[25,26,29] Recently, Liu et al.[5] reported that the cleavage of C−H bonds was greatly promoted under photocatalytic condition, which led to a new pathway of phenylmethonal oxidation on anatase TiO_2. This may provide a good evidence for the C−H bond scissor of CH_3O to form H_2CO under the photocatalytic condition, although the transformation from CH_3O into H_2CO is difficult to occur under ambient conditions.

After the formation of H_2CO, two possible reaction pathways on the $TiO_2(110)$ surface may proceed to produce $HCOOCH_3$, which can be described as follows:

$$H_2CO(a) + O_b \rightarrow HCO(a) + O_{br}H \quad (3)$$

$$HCO(a) + CH_3O(a) \rightarrow HCOOCH_3(a) \quad (4)$$

$$H_2CO(a) + CH_3O(a) \rightarrow CH_3OC(=O)H_2(a) \quad (5)$$

$$CH_3OC(=O)H_2(a) + O_b \rightarrow HCOOCH_3(a) + O_{br}H \quad (6)$$

Herein, eqs 3 and 4 for the formyl mechanism, denoted as pathway I in the following, contains an C−H scissor process to produce the intermediate HCO, and the eqs 5 and 6 for the hemiacetal mechanism, referred as pathway II, involves an initial coupling process to form the intermediate $CH_3OC(=O)H_2$. The calculated potential energy profiles of these elementary steps are shown in Figure 2b, and the data are listed in Table 2.

In pathway I for the formyl mechanism, the C−H scissor of H_2CO occurs with a large energy barrier of 2.04 eV. The corresponding atomic configuration of TS5 exhibits a strong O_{br}-H bond (0.975 Å) and the producing HCO molecule is on the way to form a hydrogen bond with nearby O_{br} atom. The electron-deficient carbonyl carbon of product HCO then attacks the electron-rich oxygen atom of CH_3O to form $HCOOCH_3$. This step undergoes an exoergic process and a

dx.doi.org/10.1021/jp505674g | J. Phys. Chem. C 2014, 118, 19859−19868

small energy barrier of 0.02 eV, which indicates that this step is an energetically and kinetically feasible.

In pathway II for the hemiacetal mechanism, the direct coupling of H_2CO and CH_3O also involves attack of the electron-rich oxygen in CH_3O by the electron-deficient carbonyl carbon of H_2CO. This step is exoergic without energy barrier, which means that the $CH_3OC(=O)H_2$ production can spontaneously occur with a high reaction rate. The $CH_3OC(=O)H_2$ species further transforms into the $HCOOCH_3$ via a C−H scissor of its H_2CO group, which needs a large energy barrier of 2.05 eV. The H transfer process of TS7 corresponds to a short O_{br}-H bond length (1.130 Å) and a long C−H bond length (1.624 Å). As a whole, the C−H scissor steps of H_2CO molecule or $CH_3OC(=O)H_2$ molecule have relatively large energy barriers in the overall oxidation process of CH_3OH into $HCOOCH_3$ via pathways I or II, demonstrating that such C−H scissor is the rate-determining step in either pathway.

Due to quite similar energy barriers for these two pathways, both pathways I and II are kinetically feasible for the oxidation of CH_3OH to $HCOOCH_3$. Thus, the key selective step between these two pathways will be dictated by the relative preference of H_2CO to produce HCO or $CH_3OC(=O)H_2$. As shown in Table 2, the $CH_3OC(=O)H_2$ production is exoergic without energy barrier, while the HCO production is largely endoergic along with a large energy barrier. This suggests that from both thermodynamic and kinetic points of view, the H_2CO prefers to form $CH_3OC(=O)H_2$ product over the HCO product. Thus, the oxidation of CH_3OH into $HCOOCH_3$ through the direct coupling of H_2CO and CH_3O should be the dominant pathway on the perfect $TiO_2(110)$, while the C−H scissor of H_2CO to produce HCO could be a secondary pathway.

3.2. Pathway of Methanol Oxidation on the Defect $TiO_2(110)$. Oxygen vacancies on the $TiO_2(110)$ surface were often regarded as the active reaction sites for catalysis and photocatalysis. Some reports have demonstrated that the CH_3OH dissociation into CH_3O could easily occur at the V_O's sites on the $TiO_2(110)$,[20,35] and such dissociation at the Ti_{5c} site could be greatly improved by the V_O's.[37] Herein, the detailed oxidation mechanism of CH_3OH into $HCOOCH_3$ on the defect surface is explored. In the (4×2) supercell, one of the bridging oxygen atoms is removed to represent the oxygen vacancy. Due to the presence of a V_O on the surface, there exist two kinds of adsorption geometries for two CH_3OH molecules on the surface: one configuration is that two CH_3OH molecules adsorb at two Ti_{5c} sites nearby the V_O; the other configuration is that one CH_3OH adsorbs at the V_O site and the other CH_3OH occupies a Ti_{5c} site. In this work, both kinds of configurations are considered.

3.2.1. Oxidation Pathway of Methanol Adsorbed at the Ti_{5c} Sites Nearby the V_O. 3.2.1.1. Adsorption of Methanol and Its Oxidation Products. As discussed above, we first considered the case that two CH_3OH molecules adsorb at two Ti_{5c} sites nearby the oxygen vacancy. Due to similar adsorption geometries of CH_3OH and its oxidation products on the perfect and defect surfaces, only the adsorption geometries of CH_3OH, HCO, and $HCOOCH_3$ on the defect surface are shown in Figure 3. It can be seen that when two CH_3OH molecules are oxidized into HCO and $HCOOCH_3$, three $O_{br}H$ are assigned to one side of the bridging oxygen row and the one $O_{br}H$ is transferred to the other side of a nearby bridging oxygen row on the defect surface. In contrast, four $O_{br}H$ are assigned equally to two nearby bridging O rows on the perfect surface, as mentioned above.

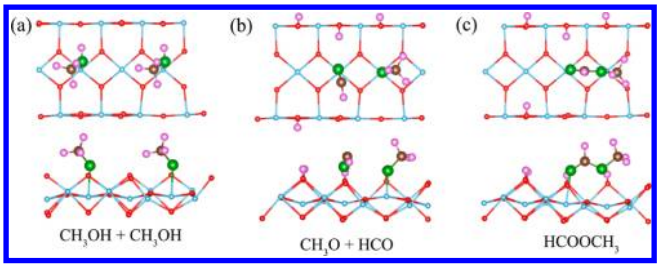

Figure 3. Top and side views of optimized adsorption structures for (a) CH_3OH, (b) CH_3O and HCO, and (c) $HCOOCH_3$ on the defect $TiO_2(110)$-(4×2) surface unit cell. The red and green represent the O atoms; light blue, gray, and purple balls represent the Ti, C, and H atoms, respectively.

The calculated adsorption energies of these molecules on the defect surface are shown in Table 1. The E_{ads} values for the CH_3OH and CH_3O are very close to those on the perfect surface, while the E_{ads} values for other molecules are more positive than those on the perfect surface. This indicates that the V_O have few effects on the adsorption of CH_3OH and CH_3O on the $TiO_2(110)$, but it makes the adsorption of other molecules on the defect surface less stable with respect to the adsorption of the corresponding molecules on the prefect surface. However, the same trend in E_{ads} among all adsorbates on both surfaces suggests that the reaction activity of each elementary step occurring at the Ti_{5c} sites is not sensitive to the surface oxygen vacancy.

It should be noted that the pure DFT calculations usually fail to describe the electronic structure of TiO_2 with oxygen vacancy. In order to know whether pure DFT can describe the other properties, the adsorption structures of CH_3OH, H_2CO, HCO, $CH_3OC(=O)H_2$ and $HCOOCH_3$ are also calculated with PBE+U. The calculated structures for each species are quite close with PBE and PBE+U. The calculated E_{ads} are 0.40 eV, 1.22 eV, 0.27 and 0.36 eV for the H_2CO, HCO, $CH_3OC(=O)H_2$, and $HCOOCH_3$, respectively. Although the adsorption energies calculated with PBE+U are more positive than the corresponding ones with PBE, the adsorption energies with PBE and PBE+U are in the same trend in the adsorption energies for these species. Thus, PBE functional is used to describe the thermodynamic and kinetic properties of adsorbates on the defect surface in the following study.

3.2.1.2. Pathways for Methanol Oxidation. The reaction mechanism of CH_3OH oxidation into $HCOOCH_3$ on the defect $TiO_2(110)$ is investigated. The overall potential profiles of all steps are illustrated in Figure 4, and the results are shown in Table 2. For the CH_3OH dissociation into CH_3O, the initial O−H dissociation step of the CH_3OH has an energy barrier of 0.34 eV, and the second O−H dissociation step exhibits a bit larger energy barrier of 0.49 eV. These energy barriers are very close to those of the corresponding steps on the perfect surface. Furthermore, the energy barrier for the C−H scissor of CH_3O into H_2CO is slightly increased by 0.17 eV relative to the reaction on the perfect surface.

For the H_2CO transformation into $HCOOCH_3$ via the formyl mechanism (pathway I), the C−H scissor step of H_2CO overcomes an energy barrier of 1.92 eV, followed by the direct coupling of HCO and CH_3O with no energy barrier. For the transformation via the hemiacetal mechanism (pathway II), the direct coupling of H_2CO and CH_3O needs an energy barrier of

dx.doi.org/10.1021/jp505674g | J. Phys. Chem. C 2014, 118, 19859−19868

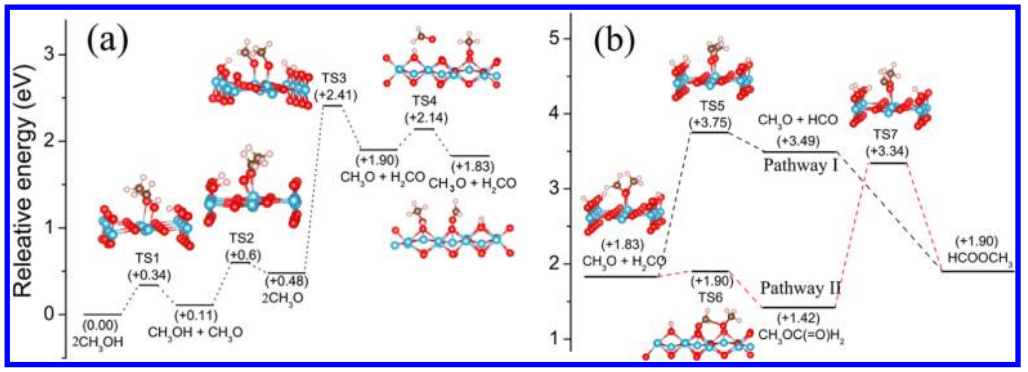

Figure 4. Calculated potential energy profile of each step for (a) CH_3OH dissociation into H_2CO and (b) H_2CO oxidation into $HCOOCH_3$ at the Ti_{5c} sites on the defect $TiO_2(110)$ (pathways I and II). The structures of the transition states in each step are embedded, and two side views of mixed H_2CO and CH_3O configuration at two adjacent Ti_{5c} sites are shown in (a) and (b) as well. Note that the energy of each configuration is relative to the total energy of the initial configuration that two CH_3OH molecules adsorb on the $TiO_2(110)$ in (a) and (b). The red, light blue, gray, and white balls in the insets represent the O, Ti, C, and H atoms, respectively.

0.07 eV, and the sequent C−H scissor step of $CH_3OC(=O)H_2$ requires an energy barrier of 1.92 eV.

As shown in Table 2, the energy barriers in all steps for pathways I and II are slightly changed on the defect surface with respect to the perfect surface. Thus, each step in the overall oxidation process of CH_3OH on the perfect and defect surfaces exhibits a quite similar reaction rate. The C−H scissors of CH_3O, H_2CO, and $CH_3OC(=O)H_2$ need to overcome the relatively large barriers in the overall oxidation process of CH_3OH, so these steps are the rate-determining steps for the overall oxidation of CH_3OH through the formyl and hemiacetal mechanisms. Due to the quite similar energy barriers in the C−H scissor steps of H_2CO and $CH_3OC(=O)H_2$ in both pathways, the dominant pathway of CH_3OH oxidation into $HCOOCH_3$ on the defect surface is still determined by the relative preference of H_2CO to produce HCO or $CH_3OC(=O)H_2$, as discussed above on the perfect surface. Thus, the oxidation of CH_3OH still proceeds through the direct coupling of H_2CO and CH_3O to produce $CH_3OC(=O)H_2$ as a dominant pathway on the defect surface.

3.2.2. Oxidation Pathway of Methanol Adsorbed at the Ti_{5c} and V_O Sites. 3.2.2.1. Adsorption of Methanol and Its Oxidation Products. To further understand the effects of surface oxygen vacancies on the oxidation mechanism of CH_3OH, we explored the oxidation process of CH_3OH adsorbed at the Ti_{5c} and V_O sites. Figure 5 shows the adsorption geometries of CH_3OH and its oxidation products, which are quite different from the aforementioned adsorption geometries on the perfect surface. The main differences arise from the adsorption of CH_3OH and CH_3O at the V_O site. The typical adsorption configuration of CH_3OH adsorbed at the V_O site is shown in Figure 5. The O atom of the hydroxyl group interacts with two Ti atoms, and the H atom of the hydroxyl group points to the nearby Ti_{5c}. Its corresponding oxidation product CH_3O remains a quite similar adsorption structure to CH_3OH, and the main difference is that the H of the hydroxyl transfers to the nearby O_{br}. The whole H_2CO molecule adsorbed at the Ti_{5c} site is parallel to the bridging oxygen row, and its oxidation product HCO becomes perpendicular to the bridging oxygen row, with its H and O atoms forming two hydrogen bonds with the O atom of CH_3O and H atom of the nearby $O_{br}H$ group, respectively. Both the $CH_3OC(=O)H_2$ and $HCOOCH_3$ sits perpendicularly to the bridging oxygen row in the [001] direction.

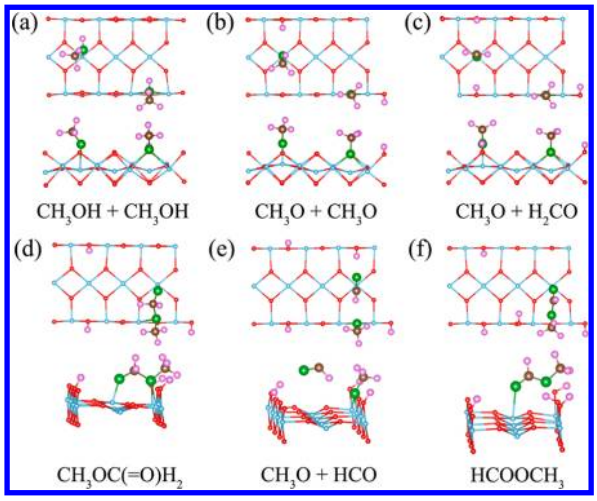

Figure 5. Top and side views of optimized adsorption structures for (a) CH_3OH, (b) CH_3O, (c) CH_3O and H_2CO, (d) $CH_3OC(=O)H_2$, (e) CH_3O and HCO, and (f) $HCOOCH_3$ on the defect $TiO_2(110)$-(4 × 2) surface unit cell. The red and green represent the O atoms; light blue, gray, and purple balls represent the Ti, C, and H atoms, respectively.

The calculated adsorption energies E_{ads} of all these species are shown in Table 1. Except for $HCOOCH_3$, all other species show more negative E_{ads} compared with those on the perfect surface, which indicate the stronger adsorption of methanol and its oxidation products on the defect $TiO_2(110)$. The more positive E_{ads} for $HCOOCH_3$ demonstrates $HCOOCH_3$ is relatively easy to desorb from the defect surface, which facilitates the overall oxidation process of CH_3OH on the surface.

It should be noted that all the species have similar change trends of E_{ads} between each other to those on the perfect surface. However, there are also two exclusive features on the defect surface. First, the more negative E_{ads} (−1.02 eV) of CH_3O at the V_O site relative to that (−0.83 eV) of CH_3OH, demonstrates that the dissociation of CH_3OH can spontaneously occur at the V_O site, as reported in previous studies.[10,20] Second, E_{ads} of H_2CO and $CH_3OC(=O)H_2$ is very close, which indicates that the direct coupling of H_2CO and CH_3O to produce $CH_3OC(=O)H_2$ is energetically unfavorable.

3.2.2.2. Pathways for Methanol Oxidation. The reaction profiles for CH_3OH oxidation into $HCOOCH_3$ adsorbed at

dx.doi.org/10.1021/jp505674g | J. Phys. Chem. C 2014, 118, 19859−19868

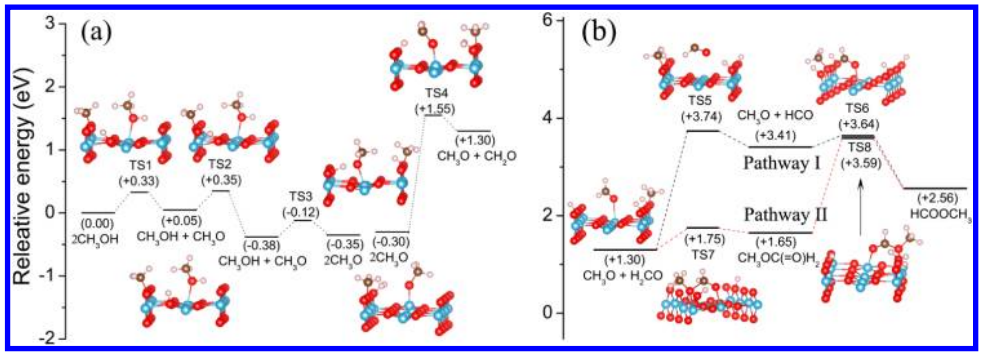

Figure 6. Calculated potential energy profiles of each step for (a) CH_3OH dissociation into H_2CO and (b) H_2CO oxidation into $HCOOCH_3$ at the Ti_{5c} and V_O sites on the defect $TiO_2(110)$ (pathways I and II). The structures of the transition states in each step are embedded in (a) and (b). Configurations of mixed CH_3OH and CH_3O adsorbed at the in-plane oxygen and Ti_{5c}, and pure CH_3O are shown in (a), mixed H_2CO and CH_3O configuration adsorbed at the adjacent Ti_{5c} and V_O sites are also shown in (b). Note that the energy of each configuration is relative to the total energy of the initial configuration that two CH_3OH molecules adsorb on the $TiO_2(110)$ in (a) and (b). The red, light blue, gray, and white balls in the insets represent the O, Ti, C, and H atoms, respectively.

both V_O and Ti_{5c} sites are investigated. The overall potential energy profiles of all relevant steps are shown in Figure 6, and the calculated results are listed in Table 2. For the initial O−H dissociation of CH_3OH at the V_O site, Oviedo et al. suggested two possible mechanisms based on their DFT calculations: one is the indirect mechanism and the other one is the direct mechanism.[35] The indirect mechanism initially forms an intermediate hydroxyl group on in-plane oxygen, and follows by the transferring of hydrogen to a neighbor O_{br}. In the direct mechanism, the main process is the hydrogen transfer from the OH group in CH_3OH to a neighbor O_{br}.

These two mechanisms of CH_3OH dissociation are both explored. The detailed reaction steps of indirect mechanism are shown in Figure 6a, and that of the direct mechanism is shown in Figure 7. The corresponding energy barriers for the indirect

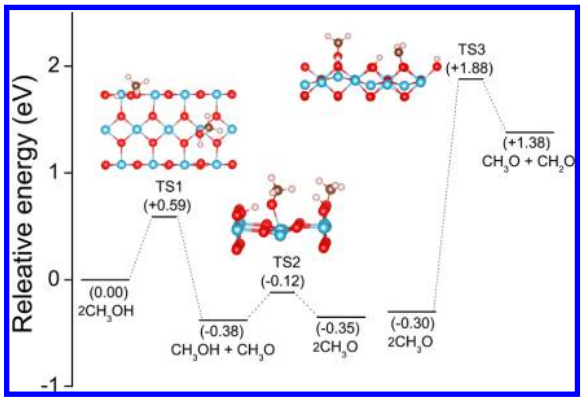

Figure 7. Calculated potential energy profiles of the relevant steps involved in the direct mechanism for CH_3OH dissociation into CH_3O and the dissociation of CH_3O into H_2CO at the V_O site on the defect $TiO_2(110)$. The structures of transition states in each step are shown as well. Note that the energy of each configuration is relative to the total energy of the initial configuration that two CH_3OH molecules adsorb on the $TiO_2(110)$. The red, light blue, gray, and white balls in the insets represent the O, Ti, C, and H atoms, respectively.

mechanism are 0.33 eV for TS1 and 0.35 eV for TS2, which is about 0.25 eV smaller than that for the direct mechanism. The result demonstrates that CH_3OH at the V_O site is facilely dissociated through the indirect mechanism.

The O−H dissociation of the second CH_3OH occurs at the Ti_{5c} site with a small endoergic energy (0.03 eV) and a small energy barrier (0.26 eV). As listed in Table 2, the energy barrier is about 0.24 eV lower than that of the corresponding step on the perfect surface or the defect surface with a bare oxygen vacancy. Such results suggest that the dissociation of CH_3OH at the V_O site can significantly promote the dissociation of the other CH_3OH at the Ti_{5c} site. This may explain the recent 2PPE observation that the photocatalytic dissociation kinetics of CH_3OH on the reduced $TiO_2(110)$ surface could be more than an order of magnitude faster than that on the perfect surface.[37]

The possible pathways of C−H scissor for CH_3O molecules into H_2CO are investigated. The corresponding reaction at the V_O is characterized by TS4 in Figure 6, and the one at Ti_{5c} is revealed by TS3 in Figure 7. The CH_3O adsorbed at the Ti_{5c} site need first orient to the opposite bridging oxygen row to dissociate at the Ti_{5c} site (see Figure 6). The dissociation of CH_3O at the Ti_{5c} site happens with an energy barrier of 1.85 eV, while the one at the V_O site needs to overcome an energy barrier of 2.18 eV. The large difference in the energy barriers for the distinct reaction sites demonstrates that the dissociation at the Ti_{5c} site is kinetically feasible.

As for the O−H breaking, the distance between H atom of the hydroxyl in CH_3OH and the nearest bridging O atom is 1.862 Å on the defect surface, smaller than the distances of 2.003 Å on the perfect surface, which leads to the relatively small energy barrier on the defect surface. As for the C−H breaking, the distance between H atom of the hydroxyl in CH_3O and the nearest bridging O atom becomes shorter about 2.497 Å on the defect surface with respect to the distance of 3.124 Å on the perfect surface, while the energy barrier on both surfaces changes slightly. Such results suggest that the O−H dissociation is greatly affected by the geometry, but C−H breaking is not sensitive to bond distance. In the previous works on photo-oxidation of water and phenylmethanol, it is also reported that O−H is affected by the geometry, while the C−H is affected by the surface hole.[5,32]

As for the formyl mechanism (pathway I), the C−H scissor of H_2CO into HCO need to overcome a large barrier of 2.44 eV. The sequent coupling between HCO and CH_3O need a low energy barrier of 0.23 eV to produce $HCOOCH_3$. In contrast, for the hemiacetal mechanism (pathway II), The direct coupling of H_2CO and CH_3O proceeds with an energy barrier of 0.45 eV to produce $CH_3OC(=O)H_2$. The following C−H scissor step of $CH_3OC(=O)H_2$ into $HCOOCH_3$ needs

dx.doi.org/10.1021/jp505674g | J. Phys. Chem. C 2014, 118, 19859−19868

to overcome an energy barrier of 1.94 eV. Compared with the corresponding energy profiles on the perfect surface or defect surface with the bare V_O, the energy barrier for $CH_3OC(=O)H_2$ production is greatly increased. The reason should originate from cleavage of two strong O−Ti bonds formed by the CH_3O adsorbed at the V_O site, and the corresponding configuration of TS7 is shown in Figure 6b.

Since the rate-determining step (i.e., the C−H scissor of the H_2CO) in pathway I for the formyl mechanism exhibits a much larger barrier than that (i.e., the C−H scissor of $CH_3OC(=O)H_2$) in pathway II for the hemiacetal mechanism, pathway II is kinetically more favorable over pathway I to produce HCOOCH3 from CH3OH on the defect surface. As a whole, the calculated energy profiles of all the relevant steps for the CH_3OH oxidation on the perfect or defect surface clearly suggest that the oxidation from CH_3OH into $HCOOCH_3$ on the $TiO_2(110)$ should be proceeded via the hemiacetal mechanism with the intermediate $CH_3OC(=O)H_2$. This strongly supports the recent supposition that the CH_3OH oxidation into $HCOOCH_3$ via the direct coupling of H_2CO and CH_3O on the reduced $TiO_2(110)$, based on the TPD and XPS measurements for the oxidation products.[28,30] In addition, the reverse reaction of intermediate $CH_3OC(=O)H_2$ production has an thermodynamic energy of about 0.4 eV on the perfect and defect $TiO_2(110)$ surfaces, as shown in Table 2. According to the Redhead formula,[47] this energy corresponds to a reaction temperature of about 150 K, which is much lower than the reported desorption temperature of formaldehyde (270 K) in the TPD spectrum.[26] Thus, it is possible that during the TPD measurements, the $CH_3OC(=O)H_2$ first dissociate into H_2CO which then desorbs from the surface. The TPD spectra only detect the desorbed product at elevated temperatures, so it is difficult to determine the production of $CH_3OC(=O)H_2$ in the methanol oxidation process. The calculated results also suggest that the intermediate might be detected by using other spectroscopy method such as Infrared spectroscopy.

3.3. Formaldehyde Diffusion on the Perfect and Defect TiO_2(110). All relevant elementary steps in the oxidation of CH_3OH into $HCOOCH_3$ involve two species on the perfect or defect surface, so it is important to evaluate the energy cost associated with diffusion on the surface and rearrangement into the starting configurations used for the above calculations. Our results demonstrate that H_2CO species binds to the perfect or defect $TiO_2(110)$ surface more weakly than CH_3O and CH_3OH, characterized by the Ti_{5c}-O bond lengths in Table 1. This is supported by the TPD measurements that the H_2CO desorbs from the $TiO_2(110)$ at lower temperature than the CH_3OH and CH_3O.[10] Thus, the H_2CO should be easier to diffuse than CH_3OH. In order to know the detailed diffusion mechanism of H_2CO, the diffusion kinetics of H_2CO along the Ti_{5c} tough toward the nearby CH_3O is explored.

The calculated energy barriers of H_2CO diffusion step on the perfect and defect surfaces are shown in Figures 2a and 4a, respectively. The configuration of transition state (TS4) is that the H_2CO molecule stays in the middle of two Ti_{5c} sites on the perfect or defect surface. The corresponding diffusion barrier is 0.24 eV on either perfect or defect surface. Such results suggest that H_2CO should diffuse freely on the surfaces to direct couple between H_2CO and CH_3O at relatively low temperature. Therefore, the reaction rates should not be limited by mass transport in the overall oxidation process of CH_3OH.

The small energy barriers for the O−H dissociation of CH_3OH on perfect or defect $TiO_2(110)$ show that CH_3OH dissociation into CH_3O can be easily initiated by thermal excitation at ambient conditions. This is quite similar to the O−H breaking of H_2O dissociation that was demonstrated to be basically a surface-catalytic reaction driven only by heat and sensitive to the surface structure of TiO_2.[32,33] In contrast, the large energy barriers for the C−H scissor of CH_3O, H_2CO and $CH_3OC(=O)H_2$ means that the oxidation of these species may occur under the photocatalytic condition. This is supported by the recent report that the C−H bond breaking can be greatly promoted by the surface hole in the photo-oxidation of phenylmethanol.[5] Thus, it is possible that the C−H bond cleavage for CH_3O, H_2CO, and $CH_3OC(=O)H_2$ may be kinetically driven by the surface hole, facilitating the overall reaction of CH_3OH oxidation into $HCOOCH_3$. It should be noted that the solvent effect is not considered in this work.

4. CONCLUSION

In summary, we have studied the mechanism for methanol oxidation into methyl formate on the perfect and defect $TiO_2(110)$ based on first-principles calculations. The calculated energy barriers of the elementary steps involved in two possible reaction pathways on the perfect surface or the defect surface with a bare bridging oxygen vacancy resolves that both pathways are kinetically feasible and the relative preference of the formaldehyde to produce the intermediate formyl or hemiacetal dictate the key selectivity-determining step between the pathways. The huge difference in the energy barriers for formyl and hemiacetal production suggests that methanol oxidation on both surfaces facilely proceeds through the intermediate hemiacetal to produce methyl formate.

Furthermore, when methanol is initially adsorbed at the oxygen vacancy, the rate-determining steps for two pathways have quite different energy barriers, which make the pathway with the intermediate hemiacetal kinetically favorable over the one with the intermediate formyl. In addition, the small diffusion barrier of formaldehyde demonstrates that formaldehyde can move freely along the Ti tough on the perfect or defect surface, which facilitates the direct coupling of methoxy and formaldehyde to produce the hemiacetal. Our finding may give new insight into the molecular-level understanding of thermal or photocatalytic reactions over TiO_2-based and help to develop a green and benign photocatalytic route for the synthesis of esters directly from alcohols or from alcohols and aldehydes.

AUTHOR INFORMATION

Corresponding Author

*E-mail: limin.liu@csrc.ac.cn.

Notes

The authors declare no competing financial interest.

ACKNOWLEDGMENTS

This work was supported by the National Natural Science Foundation of China (Nos. 51222212, 21303006), the CAEP foundation (Grant No. 2012B0302052), and the MOST of China (973 Project, Grant No. 2011CB922200).

REFERENCES

(1) Fujishima, A.; Honda, K. Electrochemical Photolysis of Water at a Semiconductor Electrode. *Nature* **1972**, *238*, 37−38.

(2) Fujishima, A.; Zhang, X.; Tryk, D. Tio2 Photocatalysis and Related Surface Phenomena. *Surf. Sci. Rep.* **2008**, *63*, 515−582.
(3) Henderson, M. A. A Surface Science Perspective on Tio2 Photocatalysis. *Surf. Sci. Rep.* **2011**, *66*, 185−297.
(4) Hansen, J.; Huo, P.; Martinez, U.; Lira, E.; Wei, Y.; Streber, R.; Lægsgaard, E.; Hammer, B.; Wendt, S.; Besenbacher, F. Direct Evidence for Ethanol Dissociation on Rutile Tio2(110). *Phys. Rev. Lett.* **2011**, *107*, 136102.
(5) Li, Y.-F.; Liu, Z.-P. Dual Reaction Channels for Photocatalytic Oxidation of Phenylmethanol on Anatase. *Phys. Chem. Chem. Phys.* **2013**, *15*, 1082−1087.
(6) Ma, Z.; et al. Photocatalytic Dissociation of Ethanol on Tio2(110) by near-Band-Gap Excitation. *J. Phys. Chem. C* **2013**, *117*, 10336−10344.
(7) Acharya, D. P.; Yoon, Y.; Li, Z.; Zhang, Z.; Lin, X.; Mu, R.; Chen, L.; Kay, B. D.; Rousseau, R.; Dohnálek, Z. Site-Specific Imaging of Elemental Steps in Dehydration of Diols on Tio2(110). *ACS Nano* **2013**, *7*, 10414−10423.
(8) Liu, L. M.; Li, S. C.; Cheng, H.; Diebold, U.; Selloni, A. Growth and Organization of an Organic Molecular Monolayer on Tio2: Catechol on Anatase (101). *J. Am. Chem. Soc.* **2011**, *133*, 7816−7823.
(9) Kominami, H.; Sugahara, H.; Hashimoto, K. Photocatalytic Selective Oxidation of Methanol to Methyl Formate in Gas Phase over Titanium(Iv) Oxide in a Flow-Type Reactor. *Catal. Commun.* **2010**, *11*, 426−429.
(10) Henderson, M. A.; Otero-Tapia, S.; Castro, M. E. The Chemistry of Methanol on the Tio2(110) Surface: The Influence of Vacancies and Coadsorbed Species. *Faraday Discuss.* **1999**, *114*, 313−329.
(11) Ahmed, A. Y.; Kandiel, T. A.; Oekermann, T.; Bahnemann, D. Photocatalytic Activities of Different Well-Defined Single Crystal Tio2surfaces: Anatase Versus Rutile. *J. Phys. Chem. Lett.* **2011**, *2*, 2461−2465.
(12) Panayotov, D. A.; Burrows, S. P.; Morris, J. R. Photooxidation Mechanism of Methanol on Rutile Tio2nanoparticles. *J. Phys. Chem. C* **2012**, *116*, 6623−6635.
(13) Chiarello, G. L.; Aguirre, M. H.; Selli, E. Hydrogen Production by Photocatalytic Steam Reforming of Methanol on Noble Metal-Modified Tio2. *J. Catal.* **2010**, *273*, 182−190.
(14) Chiarello, G. L.; Ferri, D.; Selli, E. Effect of the Ch3oh/H2o Ratio on the Mechanism of the Gas-Phase Photocatalytic Reforming of Methanol on Noble Metal-Modified Tio2. *J. Catal.* **2011**, *280*, 168−177.
(15) Henderson, M. A.; Lyubinetsky, I. Molecular-Level Insights into Photocatalysis from Scanning Probe Microscopy Studies on Tio2(110). *Chem. Rev.* **2013**, *113*, 4428−4455.
(16) Lun Pang, C.; Lindsay, R.; Thornton, G. Chemical Reactions on Rutile Tio2(110). *Chem. Soc. Rev.* **2008**, *37*, 2328−2353.
(17) Akimov, A. V.; Neukirch, A. J.; Prezhdo, O. V. Theoretical Insights into Photoinduced Charge Transfer and Catalysis at Oxide Interfaces. *Chem. Rev.* **2013**, *113*, 4496−565.
(18) Liu, L.-M.; Zhang, C.; Thornton, G.; Michaelides, A. Structure and Dynamics of Liquid Water on Rutile Tio2(110). *Phys. Rev. B* **2010**, *82*, 016415.
(19) Sun, C.; Liu, L.-M.; Selloni, A.; Lu, G. Q.; Smith, S. C. Titania-Water Interactions: A Review of Theoretical Studies. *J. Mater. Chem.* **2010**, *20*, 10319−10334.
(20) Zhang, Z.; Bondarchuk, O.; White, J. M.; Kay, B. D.; Dohnálek, Z. Imaging Adsorbate O−H Bond Cleavage: Methanol on Tio2(110). *J. Am. Chem. Soc.* **2006**, *128*, 4198−4199.
(21) Bates, S. P.; Gillan, M. J.; Kresse, G. Adsorption of Methanol on Tio2(110): A First-Principles Investigation. *J. Phys. Chem. B* **1998**, *102*, 2017−2026.
(22) Martinez, U.; Vilhelmsen, L. B.; Kristoffersen, H. H.; Stausholm-Møller, J.; Hammer, B. Steps on Rutile Tio_2(110): Active Sites for Water and Methanol Dissociation. *Phys. Rev. B* **2011**, *84*, 205434.
(23) de Armas, R. S.; Oviedo, J.; San Miguel, M. A.; Sanz, J. F. Methanol Adsorption and Dissociation on Tio2(110) from First Principles Calculations. *J. Phys. Chem. C* **2007**, *111*, 10023−10028.
(24) Zhou, C.; et al. Site-Specific Photocatalytic Splitting of Methanol on Tio2(110). *Chem. Sci.* **2010**, *1*, 575−580.
(25) Shen, M.; Henderson, M. A. Identification of the Active Species in Photochemical Hole Scavenging Reactions of Methanol on Tio2. *J. Chem. Phys. Lett.* **2011**, *2*, 2707−2710.
(26) Guo, Q.; Xu, C.; Ren, Z.; Yang, W.; Ma, Z.; Dai, D.; Fan, H.; Minton, T. K.; Yang, X. Stepwise Photocatalytic Dissociation of Methanol and Water on Tio2(110). *J. Am. Chem. Soc.* **2012**, *134*, 13366−13373.
(27) Shen, M.; Acharya, D. P.; Dohnálek, Z.; Henderson, M. A. Importance of Diffusion in Methanol Photochemistry on Tio2(110). *J. Phys. Chem. C* **2012**, *116*, 25465−25469.
(28) Guo, Q.; Xu, C.; Yang, W.; Ren, Z.; Ma, Z.; Dai, D.; Minton, T. K.; Yang, X. Methyl Formate Production on Tio2(110), Initiated by Methanol Photocatalysis at 400 Nm. *J. Chem. Phys. C* **2013**, *117*, 5293−5300.
(29) Phillips, K. R.; Jensen, S. C.; Baron, M.; Li, S. C.; Friend, C. M. Sequential Photo-Oxidation of Methanol to Methyl Formate on Tio2(110). *J. Am. Chem. Soc.* **2013**, *135*, 574−577.
(30) Yuan, Q.; Wu, Z.; Jin, Y.; Xu, L.; Xiong, F.; Ma, Y.; Huang, W. Photocatalytic Cross-Coupling of Methanol and Formaldehyde on a Rutile Tio2(110) Surface. *J. Am. Chem. Soc.* **2013**, *135*, 5212−5219.
(31) Chen, J.; Li, Y.-F.; Sit, P.; Selloni, A. Chemical Dynamics of the First Proton-Coupled Electron Transfer of Water Oxidation on Tio2 Anatase. *J. Am. Chem. Soc.* **2013**, *135*, 18774−18777.
(32) Zhao, W.-N.; Liu, Z.-P. Mechanism and Active Site of Photocatalytic Water Splitting on Titania in Aqueous Surroundings. *Chem. Sci.* **2014**, *5*, 2256−2264.
(33) Li, Y.; Liu, Z.; Gao, W. Mechanism and Activity of Photocatalytic Oxygen Evolution on Titania Anatase in Aqueous Surroundings.Pdf. *J. Am. Chem. Soc.* **2010**, *132*, 13008−13016.
(34) Li, Y. F.; Liu, Z. P. Particle Size, Shape and Activity for Photocatalysis on Titania Anatase Nanoparticles in Aqueous Surroundings. *J. Am. Chem. Soc.* **2011**, *133*, 15743−15752.
(35) Oviedo, J.; Sánchez-de-Armas, R. o.; San Miguel, M. A. n.; Sanz, J. F. Methanol and Water Dissociation on Tio2 (110): The Role of Surface Oxygen. *J. Phys. Chem. C* **2008**, *112*, 17737−17740.
(36) Zhao, J.; Yang, J.; Petek, H. Theoretical Study of the Molecular and Electronic Structure of Methanol on a Tio2(110) Surface. *Phys. Rev. B* **2009**, *80*, 235416.
(37) Zhou, C.; Ma, Z.; Ren, Z.; Mao, X.; Dai, D.; Yang, X. Effect of Defects on Photocatalytic Dissociation of Methanol on Tio2(110). *Chem. Sci.* **2011**, *2*, 1980−1983.
(38) Kresse, G.; Furthmüller, J. Efficient Iterative Schemes for *Ab Initio* Total-Energy Calculations Using a Plane-Wave Basis Set. *Phys. Rev. B* **1996**, *54*, 11169−11186.
(39) Perdew, J. P.; Burke, K.; Ernzerhof, M. Generalized Gradient Approximation Made Simple. *Phys. Rev. Lett.* **1996**, *77*, 3865−3868.
(40) Kresse, G.; Joubert, D. From Ultrasoft Pseudopotentials to the Projector Augmented-Wave Method. *Phys. Rev. B* **1999**, *59*, 1758−1775.
(41) Diebold, U.; Lehman, J.; Mahmoud, T.; Kuhn, M.; Leonardelli, G.; Hebenstreit, W.; Schmid, M.; Varga, P. Intrinsic Defects on a Tio2(110)(1 × 1) Surface and Their Reaction with Oxygen: A Scanning Tunneling Microscopy Study. *Surf. Sci.* **1998**, *411*, 137−153.
(42) Henkelman, G.; Uberuaga, B. P.; Jónsson, H. A Climbing Image Nudged Elastic Band Method for Finding Saddle Points and Minimum Energy Paths. *J. Chem. Phys.* **2000**, *113*, 9901−9904.
(43) Henkelman, G.; Jónsson, H. Improved Tangent Estimate in the Nudged Elastic Band Method for Finding Minimum Energy Paths and Saddle Points. *J. Chem. Phys.* **2000**, *113*, 9978−9985.
(44) Cant, N. W.; Tonner, S. P.; Trimm, D. L.; Wainwright, M. S. Isotopic Labeling Studies of the Mechanism of Dehydrogenation of Methanol to Methyl Formate over Copper-Based Catalysts. *J. Catal.* **1985**, *91*, 197−207.
(45) Kim, J.; Kay, B. D.; Dohnálek, Z. Formaldehyde Polymerization on (Wo3)3/Tio2(110) Model Catalyst†. *J. Phys. Chem. C* **2010**, *114*, 17017−17022.

(46) Xu, C.; Yang, W.; Guo, Q.; Dai, D.; Minton, T. K.; Yang, X. Photoinduced Decomposition of Formaldehyde on a Tio2(110) Surface, Assisted by Bridge-Bonded Oxygen Atoms. *J. Phys. Chem. Lett.* **2013**, *4*, 2668−2673.
(47) Redhead, P. A. Thermal Desorption of Gases. *Vacuum* **1962**, *12*, 203−211.